An experimental study on the comparison of crystallization behavior and structure of some Fe-B-Si-Cu-Nb and Fe-Tm-B alloys

B. Bhanu Prasad[1] and M.D.V. Srilalitha

Department of Sciences& Humanities, M.V.S.R. Engineering College, Nadergul, Hyderabad -501 510, Telangana State.

ABSTRACT

An experimental study is made to understand the crystallization behavior and structure of amorphous $Fe_{68.8}B_{9.5}$ $Si_{18.6}Cu_{0.5}$ $Nb_{2.6}$ (S1), $Fe_{73.5}$ B_9 $Si_{13.5}$ Cu_1 Nb_3 (S2), $Fe_{78}Tm_2B_{20}$ (S3) and $Fe_{76}Tm_4B_{20}$ (S4) alloys using Differential Scanning Calorimetry (DSC), X-ray Diffraction (XRD) and Scanning Electron Microscopy (SEM). DSC curves of amorphous $Fe_{68.8}B_{9.5}$ $Si_{18.6}Cu_{0.5}$ $Nb_{2.6}$ (S1)and $Fe_{73.5}$ B_9 $Si_{13.5}$ Cu_1 Nb_3 (S2) showed two-step crystallization. A wide region that occurs between the two crystallization stages ensures the useful properties of the material before boride formation. Comparing these results with XRD results, these two peaks represent the growth of the crystalline phases of α-Fe(Si) at peak 1 and Fe_3Si at peak 2. In amorphous $Fe_{78}Tm_2B_{20}$ (S3) and $Fe_{76}Tm_4B_{20}$ (S4) alloys, the crystallization is a multi-stage process where different crystalline phases grow in the amorphous matrix. Our study shows that when Tm 2% and 4% are added to Fe-B alloys, the crystallized ribbons consists of α-Fe and Fe_3B.

KEYWORDS: DIFFERENTIAL SCANNING CALORIMETRY, X-RAY DIFFRACTION, CRYSTALLINE PHASES, AMORPHOUS FERROMAGNETS.

INTRODUCTION

Amorphous ferromagnetic ribbons, made by melt spinning technique are fascinating class of metallic materials that do not display long range atomic order. Due to their amorphous character , these materials exhibit excellent soft, hard, electrical and mechanical properties [1- 8]. These properties include very high saturation magnetization (~1.3T), low coercivity H_c (~0.5Am^{-1}), low saturation magnetostriction (~2x10^{-6}) and high effective permeability μ(~10^5). Copper promotes the nucleation of the bcc grains, while Niobium hinders their growth and at the same time inhibits the formation of boride compounds [8, 9]. It is well known that Fe-based nano crystalline alloys are used in several commercial applications including power devices, power electronics, telecommunications, information handling, and magnetic sensors. They are indispensable in many applications in magnetic parts and devices such as inductors, low and high energy frequency transformers alternating current machines, motors, generators and sensors [10 - 12].

In this paper we present the crystallization behavior and structure of amorphous $Fe_{68.8}B_{9.5}$ $Si_{18.6}Cu_{0.5}$ $Nb_{2.6}$ (S1), $Fe_{73.5}$ B_9 $Si_{13.5}$ Cu_1 Nb_3 (S2), $Fe_{78}Tm_2B_{20}$ (S3) and $Fe_{76}Tm_4B_{20}$ (S4) alloys. The results are compared and discussed.

EXPERIMENTAL

Amorphous $Fe_{68.8}B_{9.5}$ $Si_{18.6}Cu_{0.5}$ $Nb_{2.6}$ (S1) and $Fe_{73.5}$ B_9 $Si_{13.5}$ Cu_1 Nb_3 (S2), $Fe_{78}Tm_2B_{20}$ (S3) and $Fe_{76}Tm_4B_{20}$ (S4) alloy ribbons were made using melt spinning technique which are procured from our other researchers. The width of these ribbons vary from 1 mm to 10 mm and their width is about 30 μm. Differential Scanning Calorimetry (DSC) measurements were made in the temperature range 30^0C – 1000^0C. Structure of the samples were examined on the MAXIMA_X 7000 XRD SERIES X-Ray diffractometer with the HZG-3 goniometer and computerized reflected radiation recording system, equipped with the cobalt anode lamp, with 40 kV voltage and with 20 mA heater current. For the fresh and annealed samples, X-ray diffraction patterns are recorded at room temperature.

RESULTS AND DISCUSSION

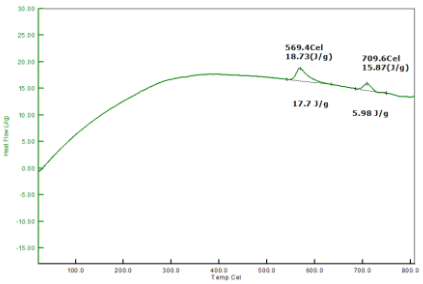

(a)

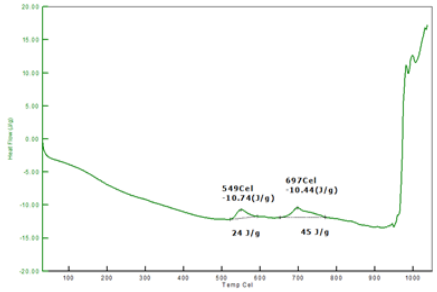

(b)

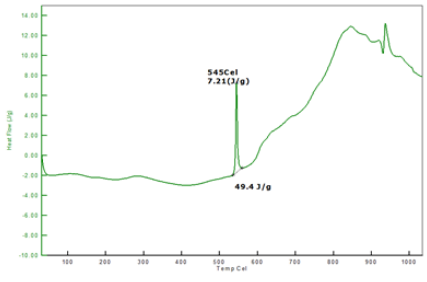

(c)

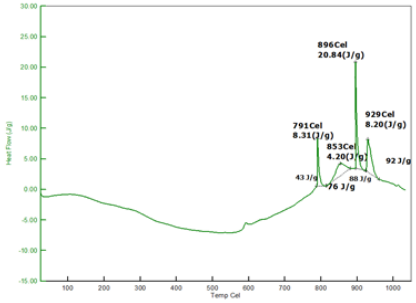

(d)

Figure 1 DSC curves of amorphous (a) $Fe_{68.8}B_{9.5}$ $Si_{18.6}Cu_{0.5}$ $Nb_{2.6}$ (S1), (b) $Fe_{73.5}$ B_9 $Si_{13.5}$ Cu_1 Nb_3 (S2), (c) $Fe_{78}Tm_2B_{20}$ (S3) and (d) $Fe_{76}Tm_4B_{20}$ (S4) alloys at a heating rate of 20°C/min

Figure 1 shows a high temperature DSC curves of amorphous $Fe_{68.8}B_{9.5}$ $Si_{18.6}Cu_{0.5}$ $Nb_{2.6}$ (S1) and $Fe_{73.5}$ B_9 $Si_{13.5}$ Cu_1 Nb_3 (S2), $Fe_{78}Tm_2B_{20}$ (S3) and $Fe_{76}Tm_4B_{20}$ (S4) alloys recorded at a heating rate of 20^0C/min in the temperature range 30^0C - 800^0C. Two peaks are observed i.e., first peak at 569.4^0C and second peak 709.6^0C. It reveals that the alloy undergoes two stage crystallization reactions at 569.4^0C and 709.6^0C. This gives wide temperature interval of 140.2^0C between two crystallization stages.

As shown in Fig.1 (a), the first broad peak in the present case arises due to (1) Structural relaxation occurring with a broad range of relaxation times due to a variety of atomic rearrangement and (2) Formation of intermediate metastable phases. The second peak arises due to crystallization which is a defined nucleation and growth reaction. Broadening also occurs due to kinetic reasons as the kinetics involving structural processes slows down due to the disappearance of free volume during relaxation processes. As in Figure1(b), amorphous sample S2 shows two crystalline peaks, first peak at 549^0C (822 K) and second peak at 697^0C (970 K). Thus, it reveals that the alloy undergoes two stage crystallization reactions. This gives wide temperature interval of 14^08C between two crystallization stages. Observation of two step crystallization is more common in metallic glasses contained more than three elements than in those containing less components. Two well-defined exothermic peaks may correspond to two different crystallization phases of namely, α-Fe(Si) and Fe_2B phases.

Figure 1 (c)shows the DSC curve of fresh amorphous S3. On heating the sample up to 1000^0C, a sharp peak was observed at 545^0C, indicating a primary crystalline phase appearing in the amorphous matrix. Another sharp peak was observed at higher temperatures showing further crystallization of the sample. Minor peaks are observed around 853^0C and 929^0C. The sample is completely crystallized after 950^0C. Thus, in sample S3, the crystallization is a multi-stage process where different crystalline phases grow in the amorphous matrix. Figure 1 (d) shows the DSC curve of fresh amorphous sample S4. Thus, DSCcurve of sample S4 shows a sharp peak at 791^0C indicating a primary crystalline phase appearing in the amorphous matrix. Another sharp peak was observed at higher temperatures showing further crystallization of the sample. Further heating of the sample showed a small broad peak at 853^0C, a sharp peak at 896^0C and a slightly sharp at 929^0C. The sample is completely crystallized after 929^0C. Thus, in sample S4, the crystallization is also a multi-stage process where different crystalline phases grow in the amorphous matrix.

Thus, the transformation from amorphous state into the crystalline one takes place typically in more than one stage – at first the ferromagnetic phases crystallizes, and subsequently the evolution of borides phases from the remaining amorphous matrix appears. After the study of all the samples (S1 – S4), we can conclude that soft ferromagnetic amorphous alloys and hard ferromagnetic amorphous alloys show two stage crystallization and certain phases are existing at higher temperatures. Thus, Table 1 gives the information of the peak temperatures of all the samples together.

For sample S4, peak 3 and peak 4 are observed at 896 K and 929 K, respectively where enthalpy phases transformation is 20.84 j/g and 8.20 j/g respectively.

In the DSC curve of the samples S1 and S2, the first peak corresponds to the formation of α-Fe(Si) phase while the second one corresponds to the formation of the Fe_3Si where as in samples S3 and S4, the first peak corresponds to the formation of α-Fe and the second peak corresponds to Fe2B compounds [13 -16]. A large separation of the two

crystallization stages (about 140 K) in $Fe_{68.8}B_{9.5}$ $Si_{18.6}Cu_{0.5}$ $Nb_{2.6}$ (S1) and $Fe_{73.5}$ B_9 $Si_{13.5}$ Cu_1 Nb_3 (S2) shows another feature of alloys exhibiting easy Nano crystallization. It is well known that Cu additions to Fe–Si–B–Nb glasses broadens the peak and the crystallization temperature of the Nb and B-enriched amorphous phase [17, 18]. This is because there is no attractive interaction between Cu and Nb and no driving force for alloying or compound formation. Thus, Cu additions to amorphous Fe-based alloys containing Nb atoms will have tendency to phase-separate out of the matrix facilitating a high density of crystal formation[19]. Additions of Cu and Nb together with higher broadening of the peaks are thus favorable to soft magnetic properties. With both Cu and Nb alloying additions, the DSC thermograms of sample 1 and sample 2 alloys is flatter and wider than those found in other alloys, suggesting lower crystallization kinetics which may be due to a substantial decrease in the crystal growth rate [20]. Previous investigations determined that the amorphous- crystalline transition in Fe-B alloys begins with the precipitation of α-Fe and Fe_3B, then metastable Fe_3B decomposes to α-Fe and Fe_2B[5.9]. Our study shows that when Tm 2% and 4% is added to Fe-B alloys, the crystallized ribbons consist of α-Fe and Fe_3B which was confirmed by XRD studies.

Table 1
Peak temperatures and Enthalpy phases transformation of the samples S1 – S4.

Sample	Peak temperatures		Enthalpy phases transformation	
	Peak 1 (^{0}C)	Peak 2 (^{0}C)	Peak 1(j/g)	Peak 2 (j/g)
$Fe_{68.8}B_{9.5}$ $Si_{18.6}Cu_{0.5}$ $Nb_{2.6}$ (S1)	569.4	709.6	18.73	15.87
$Fe_{73.5}$ B_9 $Si_{13.5}$ Cu_1 Nb_3 (S2)	549.0	697.0	10.74	10.44
$Fe_{78}Tm_2B_{20}$ (S3)	545.0	----	7.21	---
$Fe_{76}Tm_4B_{20}$ (S4)	791.0	853.0	8.31	4.20

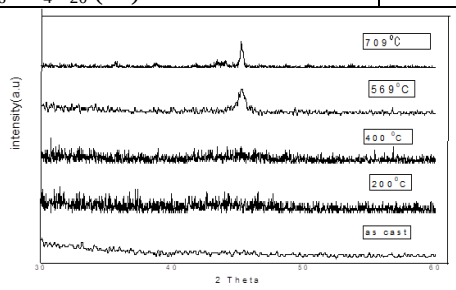

(a)

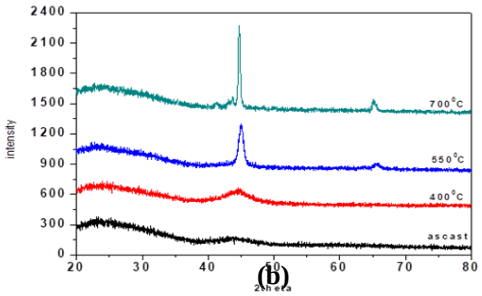

(b)

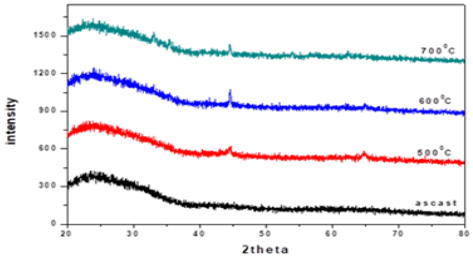

(c)

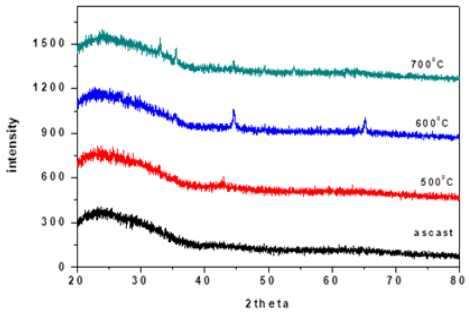

(d)

Figure 2 X-Ray diffraction pattern (XRD) of the as received and heat treated samples of amorphous (a) $Fe_{68.8}B_{9.5}$ $Si_{18.6}Cu_{0.5}$ $Nb_{2.6}$ (S1), (b) $Fe_{73.5}$ B_9 $Si_{13.5}$ Cu_1 Nb_3 (S2), (c) $Fe_{78}Tm_2B_{20}$ (S3) and (d) $Fe_{76}Tm_4B_{20}$ (S4) alloys

In the present study X-ray diffraction technique has been used to identify the crystalline phases as well as the grain size of the different samples by using Debye Scherrer's formula [5.16] given by

$$D = 0.94\lambda / Cos\theta \quad \ldots\ldots\ldots\ldots(1)$$

where D is the grain size, β is the full width at half maximum (FWHM), θ is the angle of diffraction and λ is the wave length of Cu-Kα radiation.

The XRD pattern of the as-cast alloy is shown at the bottom of the figure in each sample. Presence of broad band reveals the amorphous nature of the sample. The samples heat treated at different temperatures reveals emergence of few peaks in XRD pattern and analysis indicate that some phases are present at those temperatures. From the XRD analysis the grain size of the grown crystalline phases for all the samples (S1 – S4) is calculated and compared.

XRD spectra of amorphous $Fe_{68.8}B_{9.5}Si_{18.6}Cu_{0.5}Nb_{2.6}$ (S1) and $Fe_{73.5}B_9Si_{13.5}Cu_1Nb_3$ (S2) $Fe_{78}Tm_2B_{20}$ (S3) and $Fe_{76}Tm_4B_{20}$ (S4) alloys shown in Fig. 2 clearly confirm that the as cast samples in the amorphous state. The XRD pattern of the sample S1 annealed at 200^0C and 400^0C for one hour indicates slightly a different behaviour but still can be attributed with no major changes in the amorphous nature. It refers that the crystallization has not yet been started at those temperatures. For the fresh samples annealed at 569^0C and 709^0C, a peak is observed around $2\theta = 45^0$ which may be due to the presence of α-Fe(Si). The grain size of the grown crystalline phase for the annealed sample at 569^0C is about 18.9 nm. Similarly, the grain size of the grown crystalline phase for the annealed sample at 709^0C is about 45.4 nm {Table 2]. This shows that as the annealing temperature increases the grain size increases.

Figure 2(b) shows XRD pattern ofS2 sample as received and after annealing at different temperatures. It is found that α-Fe(Si) phase (Peak 1) appears clearly without any other phase annealed at 400^oC. At higher temperatures, another phase Fe_3Si appears (Peak 2) at 550^oC. The phases α-Fe(Si) and Fe_3Si atPeak 1 and Peak 2, respectively become evident when the annealing temperature is raised to 700^oC. The grain size of the grown crystalline phase for the annealed sample at 400^0C is about 3.5 nm. The grain size of the grown crystalline phases for the annealed sample at 550^0C is about 10 nm and 7.68 nm for Peak 1 and Peak 2 (Fig. 2b), respectively. Similarly, the grain size of the grown crystalline phases for the annealed sample at 700^0C is about 26.3 nm and 18.8 nm, respectively [Table 2]. This shows that here also as the annealing temperature increases the grain size ncreases. It is reported that in the crystallization behavior of $Fe_{72.5}Cu_1Nb_{4.5}Si_10B_{12}$, $Fe_{73.5}B_9Si_{13.5}Cu_1Nb_3$ (S2) and $Fe_{72}Cu_1Nb_{4.5}Si_{13.5}B_9$ alloys after primary crystallization, the α-Fe(Si) phase was formed for the alloy which has 10 at.% Si. The ordered $Fe_{80}Si_{20}$ phase was formed for alloys containing 13.5 at.% Si. The $Fe_{73.5}B_9Si_{13.5}Cu_1Nb_3$ alloy (S2) exhibited superior soft magnetic properties among the measured alloys when annealed about 602^0C for 30 min. The rapid deterioration in the magnetic properties at higher temperatures of the annealed alloys was primarily due to the formation of the Fe_2B phase, which has a strong magnetocrystalline anisotropy energy.

When amorphous ribbons of $Fe_{73.5}B_9Si_{13.5}Cu_1Nb_3$ alloy has been annealed in the temperature range 475^0C – 700^0C, crystallization induced by heat treatment resulted in the formation of α-(Fe-Si) phase. The phase formed by primary crystallization has been found to be Fe-Si solid solution with a composition corresponding to disordered Fe-Si. Secondary crystallization of the Fe_3B and Fe_2B phases arises with the individual branches at the interfaces of the closely packed crystals at the temperature 680^0C, the spacing of such crystals was of the order of nanometer.

The grain sizes of the observed crystalline phases of samples S1 and S2, deduced from the XRD data using the Scherrer formula, calculated by us, are in good agreement with those values of similar samples reported in the literature [17-21]. It is also reported that the annealings gave rise to excellent soft magnetic properties which correspond to those Co-based amorphous alloys. Especially, the alloys containing Cu and Nb were superior to the alloys containing other elements. These new alloys were composed of Ultrfine grain structure. The grains were about 10 nm in diameter and the main crystalline phase presumed to be a bcc Fe solid solution which contains Si and B. This might be attributed to the nucleation process of the bcc Fe-Si-B solid solution influenced by Cu and the suppression of the grain growth by Nb. The newly developed alloys are suitable for many kinds of magnetic components such as saturable reactors, choke coils and transformers, because of their excellent soft magnetic properties and high saturation flux density. The soft magnetic properties are substantially improved by the simultaneous addition of Cu and Nb. In the crystallized $Fe_{73.5}B_9Si_{13.5}Cu_1Nb_3$ alloy (S2), new crystalline phases, tetragonal Fe_3B and hexagonal Fe_2Si (not reported previously) exist in all the nanocrystalline alloys in question in contrast to well-documented cubic Fe-Si phase with the DO_3 structure which coexists with the Fe_3B and Fe_2Si phases in some compositions only. The crystallization of Fe_3B and Fe_2Si nanocrystalline grains starts at the surface of the ribbons and then proceeds to the bulk whereas the crystallization of DO_3Fe-Si gets initiated in the bulk itself. The average size of the nanocrystalline grains of the Fe_3B and Fe_2Si and cubic DO_3 Fe-Si structures in the residual amorphous matrix is around 20 nm.

It is also reported that in Fe-Cu-Nb-Si-B alloys, the primary crystalline phase is α-Fe(Si). It changes to Fe_3Si (DO_3) on increasing the Si content.

Thus, we conclude that for the samples of $Fe_{73.5}B_9Si_{13.5}Cu_1Nb_3$ alloy (S2) that we have studied, the XRD results confirm that two crystalline phases namely, α-Fe(Si) and Fe_3Si grow in the

annealed samples and their grain sizes increase with increase in the annealing temperature.

Figure 2 shows the XRD patterns of amorphous $Fe_{78}Tm_2B_{20}$ alloy (S3) for the as cast and annealed samples at different temperatures. The XRD pattern of the as cast sample shows the amorphous nature of the sample. XRD pattern of the sample annealed at 500^0C shows twominor peaks for $2\theta=45^0$ and $2\theta=65^0$, respectively. These peaks arise due to the growth of the crystalline phases α-Fe and Fe2B in the annealed sample. Thus, XRD patterns of the fresh sample (S3) annealed at temperatures 600^0C and 700^0C clearly indicate the presence of α-Fe.

Similarly, Fig.2 also shows the XRD patterns of amorphous Fe76Tm4B20 alloy (S4), annealed at different temperatures which confirms the presence of α-Fe and Fe_2B phases in the annealed samples. Thus, in general, Fe-Tm-B amorphous alloys may show the presence of α-Fe and Fe_2B phases in the annealed samples.

Table 2
Grain size (in nm) of the phases of the samples (S1 – S4) annealed at different temperatures

Sample	At 400°C		At 550°C		At 700°C	
	Peak 1	Peak 2	Peak 1	Peak 2	Peak 1	Peak 2
$Fe_{68.8}B_{9.5}$ $Si_{18.6}Cu_{0.5}$ $Nb_{2.6}$ (S1)	---	---	18.9	--	45.4	---
$Fe_{73.5}$ B_9 $Si_{13.5}$ Cu_1 Nb_3 (S2)	3.5	---	107.68	26.3	18.8	---
Sample	**AT 500°C**		**At 600°C**		**At 700°C**	
	Peak 1	**Peak 2**	**Peak 1**	**Peak 2**	**Peak 1**	**Peak 2**
$Fe_{78}Tm_2B_{20}$(S3)	11.9	11.4	15.8	17.3	17.5	----
$Fe_{76}Tm_4B_{20}$ (S4)	----	----	14.7	17.0	16.4	17.1

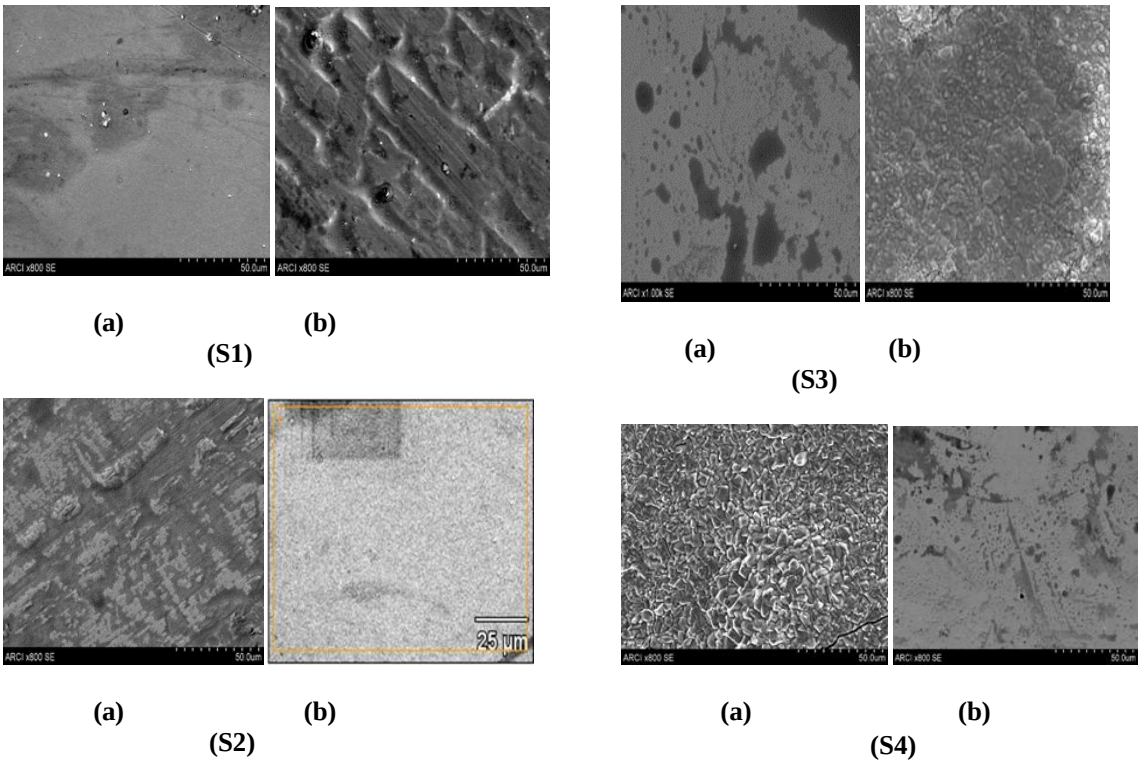

Figure 3 SEM photos of amorphous $Fe_{68.8}B_{9.5}$ $Si_{18.6}Cu_{0.5}$ $Nb_{2.6}$ (S1), $Fe_{73.5}$ B_9 $Si_{13.5}$ Cu_1 Nb_3 (S2),$Fe_{78}Tm_2B_{20}$ (S3) and $Fe_{76}Tm_4B_{20}$ S4)alloysbefore (a) and after (b) heating.

In sample S4, annealed at 700^0C, At Peak 3 showed the grain size 20.6 nm.

By using scanning electron microscope (SEM) micro structural studies were carried out. Thus, Figure 3 shows the SEM images of amorphous $Fe_{68.8}B_{9.5}$ $Si_{18.6}Cu_{0.5}$ $Nb_{2.6}$ (S1), Fe73.5Cu1Nb3Si13.5B9 (S2), Fe78Tm2B20(S3) and Fe76Tm4B20 (S4) alloys, before and after heating.

The heated samples show a type of Dendrite structure, which is a typical microstructural phase. Thus, sample S1 and S2 show α-Fe(Si), in the crystallized samples. This observation is consistent with the XRD results. This proves that thermal crystallization involves the primary crystallizationα-Fe(Si), and the eutectic crystallization Fe_3Si as discussed in XRD results. As in Figures 3, SEM micrographs of samples S3 and S4 show amorphous nature before heating and after heating, SEM micrographs of the samples S3 and S4 show the primary crystallization α-Fe phase and the eutectic crystallization Fe_2B as discussed in XRD results.

CONCLUSIONS

Peaks shown in the DSC curves of the samples corresponds to the formation of α-Fe(Si) and Fe_3Si phases in the samples S1 and S2 while the peaks in the DSC curves of samples S3 and S4 corresponds to the formation of α-Fe and Fe_2B phases which are confirmed by XRD and SEM studies in the crystallized samples.

ACKNOWLEDGEMENTS

Authors would like to thank the Management members of Matrusri Education Society (MEC), Principal, HOD, Faculty and Staff of Sciences & Humanities for their continuous support and encouragement in completing this work.

REFERENCES

[1] C.A. Schuh, T.C. Hufnagel and U. Ramamurty, Acta Mater. 55 (2007) 4067
[2] A.L. Greer, Y.Q. Cheng, and E. Ma, Mater. Sci. Eng. R 74(2013) 71.
[3] C. Suryanarayana and A. Inoue, Int. Mater. Rev. 58 (2013) 131
[4] L. Xia, K.C. Chan and M.B. Tang, J. Alloys Compd. 509(2011) 6640.
[5] M. Zhao, K. Abe, S.I. Yamaura, Y. Yamamoto and N. Asao, Chem. Mater. (2014) 1056
[6] A. Inoue, X.M. Wang and W. Zhang, Rev. Adv. Mater. Sci. 18(2008) 1
[7] Akihisa Inoue and Nobuyuki Nishiyama, MRS Bulletin, 32 (2007) pp. 651-658
[8] J.S. Dugdale and D. Pavuna, Endeavour, 9 (1985) pp. 62-66
[9] Y. Naitoh, T. Bitoh, T. Hatanai and A. Makino, J. Appl. Phys. 83 (1998) 6332
[10] Akhiro Makino and TeruoBitoh, J. Appl. Phys., 81(1997) 2736
[11] A. Makino, A. Inoue and T. Masumoto, Mat. Trans, JIM, 36 (1995) 924
[12] K. Hono, K. Hiraga, Q. Wang, A. Inoue and T. Sakurai, Acta Metall. et Mat. 40 (1992) 2137
[13] A.R. Bhatti and B. Cantor, J. Mater. Sci. 29 (1994) 816.
[14] K. Chrissafis, M.I. Maragakis, K.G. Efthimiadisand E.K.Polychroniadis J. Alloys Compd. 28 (2004) 375.
[15] K.G. Efthimiadis, E.K. Polychroniadis, S.C. Chadjivasiliouand I.A.Tsoukalas, Mater. Res. Bull. 35 (2000) 937.
[16] K.G. Efthimiadis, G. Stergioudis, S.C. Chadjivasiliouand I.A.Tsoukalas, Cryst. Res. Technol. 37 (2002) 827.
[17] I. Matko, P. Duhaj, P. Svecand D.Janickovic, Mater. Sci. Engg., A 179/180 (1994) 557.
[18] F. Zhou, K.Y. He and M.L. Sui, Mater. Sci. Engg., A 181/182 (1994) 1419.
[19] J.D. Ayers, V.G. Harris, J.A. Sprague and W.T. Elam, Appl. Phys. Lett.64 (1994) 974.
[20] Y.R. Zhang and R.V. Ramanujan, Thin Solid Films 505 (2006) 97